CHARACTERIZATION OF DISRUPTION PHENOMENOLOGY IN ITER

R. YOSHINO[1], D.J. CAMPBELL[3], E. FREDERICKSON[4], N. FUJISAWA[2], R. GRANETZ[5], O. GRUBER[6], T.C. HENDER[7], D.A. HUMPHREYS[9], N. IVANOV[8], S. JARDIN[4], A.G. KELLMAN[9], R. LAHAYE[9], J. LISTER[10], S. MIRNOV[11], A.W. MORRIS[7], Y. NEYATANI[1], G. PAUTASSO[6], F.W. PERKINS[2], S. PUTVINSKI[2], M.N. ROSENBLUTH[2], N. SAUTHOFF[4], S. TOKUDA[1], P. TAYLOR[9], T. TAYLOR[9], K. YAMAZAKI[12], J. WESLEY[2]

[1]JAERI, Naka, Ibaraki, Japan; [2]ITER Joint Central Team; [3]The NET Team, Garching, Germany; [4]PPPL, Princeton, NJ, USA; [5]Plasma Fusion Center, MIT, MA, USA; [6]Max-Planck IPP, Garching, Germany; [7]Euratom/UKAEA, Culham, Abingdon, UK; [8]Kurchatov Institute, Moscow, RF; [9]General Atomics, San Diego, USA; [10]CRPP, Lausanne, Switzerland; [11]TRINITI, Moscow, Russian Federation; [12]NIFS, Toki, Japan

Abstract
Characterization of disruption phenomenology in support of the ITER design is described.

1. INTRODUCTION

Disruptions terminate tokamak discharges by thermal quench and current quench. Vertical instability, in-vessel halo currents and conversion of plasma current to runaway electron current typically follow. In ITER, disruptions and their consequences have implications for the design of the first wall, divertor targets and torus vacuum vessel. This paper summarizes disruption, halo current and runaway electron data compiled by the ITER Expert Group on Disruption, Plasma Control and MHD to support ITER design. Methods for avoiding disruptions or for mitigating their consequences have also been assessed. There is progress in the characterization and avoidance/effect-mitigation studies, and disruption avoidance and effect mitigation methods have been demonstrated in present experiments.

2. THERMAL AND CURRENT QUENCH

Thermal quenches are often observed to take place in two stages (Fig. 1 inset) [1]. Single-stage thermal quenches are also observed, sometimes on slower time-scale, presumably due to overlap of two stages [2]. In the first stage, m=1/n=1 erosion of central temperature takes place, but the plasma outside the q=2 surface still acts as a thermal barrier, so only a fraction of the total thermal energy is lost. In the second stage, the thermal barrier breaks down and the remaining thermal energy is lost to the wall. Thermal quench times are plotted against minor radius in Fig. 1. Although the data are scattered, the initial delay time $\tau_{1\text{-}2}$ and the fast quench time τ_2 increase with scalings $a^{1.5}$ and a^1, respectively. Extrapolation to ITER (a =2.8 m) yields $\tau_{1\text{-}2} \approx 20$ ms and $\tau_1 \approx 1$ ms.

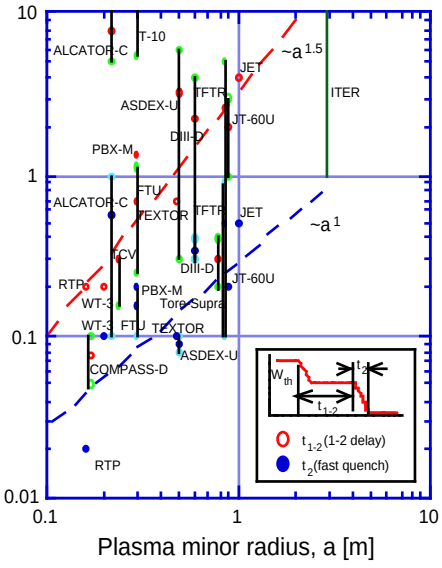

FIG. 1. Thermal quench times for various tokamaks, plotted vs. plasma minor radius.

For current quench, the first design consideration is the rate of current decay, which determines EM loading by toroidal eddy currents. Current decay rate also enters into setting the magnitude of halo currents. Slower current quenches lead to higher halo currents, so estimate of maximum and minimum decay rate in ITER is required. Current quench data has been obtained from various tokamaks as shown in Fig. 2. Current quench times Δt_{cq} divided by the plasma cross section S are plotted as a function of the pre-disruption current density $J_{p0} = I_{p0}/S$. Here S is the pre-disruption cross-section area and Δt_{cq} is corrected to the 60% linear decay time (time for 60% drop in plasma current). Minimum $\Delta t_{cq}/S$ is 0.8 ms/m^2: this corresponds to 32 ms for 60% current decay and 53 ms for 100% decay in ITER. The $\Delta t_{cq}/S$ scaling in Fig. 2 is consistent with impurity radiation cooling. When power balance between joule heating and impurity radiation with coronal equilibrium is assumed, $\Delta t_{cq}/S$ is a function of electron temperature T_e and current density J_{p0}. Lines of 2, 5 and 8 eV in Fig. 2 are estimated for 10% carbon impurity and

plasma internal inductance l_i = 0.7. The lower bound of $\Delta t_{cq}/S$ corresponds to an average temperature T_e = 3~5 eV.

Figure 2 shows that slower decay rates, corresponding to higher T_e, comprise most of the data. The ratio of maximum to minimum rate is about 20. For ITER the slowest current decay time will be about 1 s, which is longer than the vertical instability growth time (~ 0.5 s). Hence slow current quenches in ITER will produce VDEs with higher halo currents.

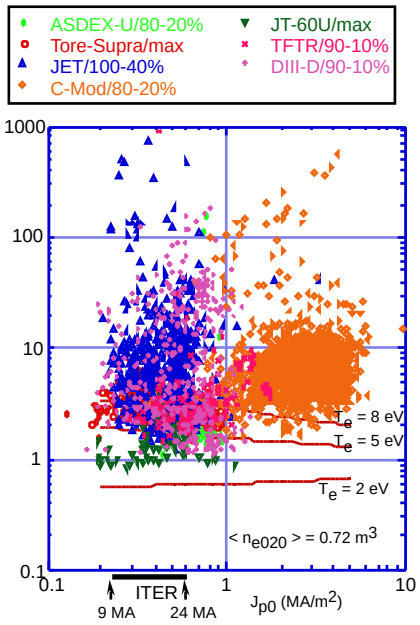

FIG. 2. Current quench time normalized by plasma cross section vs. plasma current density.

3. HALO CURRENT

In-vessel poloidal (halo) currents occur in elongated tokamaks following disruption or loss of equilibrium control. Figure 3 shows data from various tokamaks, where toroidal peaking factors T_{pf} are shown for maximum halo current $I_{h,max}$ normalized by initial plasma current I_{p0}. Higher peaking factors are seen only at lower $I_{h,max}/I_{p0}$. From Fig. 3 $I_{h,max}/I_{p0} \leq 0.4$ (≤ 0.25 typical), $1.2 \leq T_{pf} \leq 4$, and $(I_{h,max}/I_{p0}) \times T_{pf} \leq 0.75$ (0.50 typical) are recommended as the design basis for ITER. Structural loadings from this basis can be accommodated with adequate engineering margins. Dependence of $I_{h,max}/I_{p0}$ and T_{pf} on plasma size (R or a) has not been clarified, but data in JET [4] and JT-60U [5] show $I_{h,max}/I_{p0} \leq 0.25$-$0.3$ and $(I_{h,max}/I_{p0}) \times T_{pf} \leq 0.52$ (Fig. 4). This suggests larger tokamaks (and ITER) may have lower halo current fraction and T_{pf}. In JT-60U, $(I_{h,max}/I_{p0}) \times T_{pf}$ decreases with the increase in plasma current and plasma stored energy [5].

The cause for halo current asymmetry is not fully understood. The potential for VDE plasmas to be kink unstable in the final q 1 phase is clear. A model based on non-linear kink instability shows that T_{pf} should decrease with increase in $I_{h,max}/I_p$ [6]. The T_{pf} variation in Fig. 3 is in qualitative

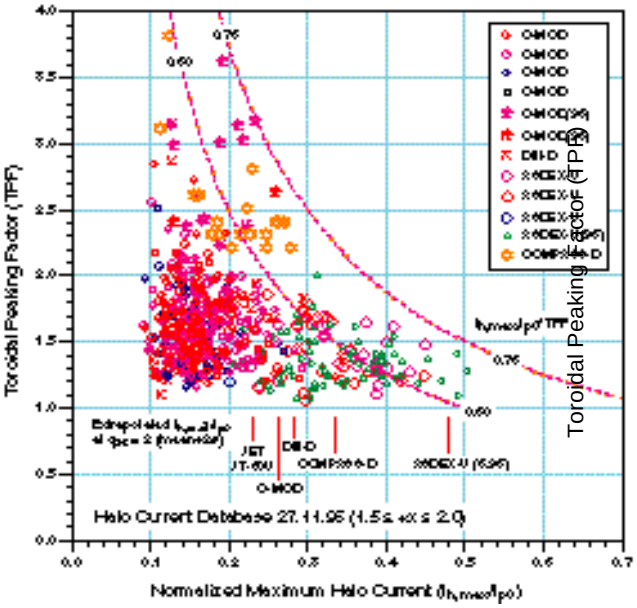

FIG.3. Toroidal peaking of halo currents vs. $I_{h,max}/I_{p0}$ Bounds for maximum $I_{h,max}/I_{p0}$ at q_{95} =3 are also shown

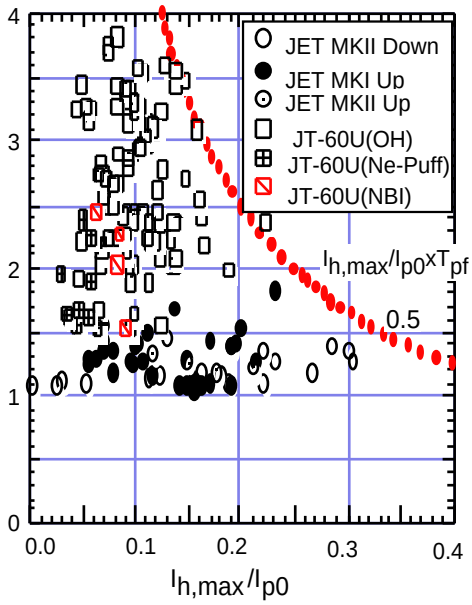

FIG.4. T_{pf} versus $I_{h,max}/I_{p0}$ in JET and JT-60U. JT-60U data for $1.3 \leq \kappa_X \leq 1.5$.

agreement with this model. Alternately, toroidal asymmetry in JET is correlated with a tilted/radially-displaced plasma column [4] and instability of the halo current stemming from the reshaping of the current path is also proposed as a mechanism to enhance T_{pf} [7]. Given these varying interpretations, projection of $I_{h,max}/I_{p0}$ and T_{pf} for ITER remains based on the empirical data in Figs 3 and 4.

4. DISRUPTION FREQUENCY

Causes of disruptions are i) occurrence of plasma MHD instabilities, ii) operational problems with the plasma control system or human mistakes, and iii) intentional plasma shutdown for machine protection (8]. Disruption 'prediction' systems can minimize disruptions caused by i), and fast plasma shutdown methods are proposed to mitigate the effects of disruptions in general and to make category iii) disruptions acceptable. For categories i) and ii), low disruption frequency (~ 1%) is possible with reliable hardware and well-developed discharges, including 'high-performance' discharges. However, higher disruption frequency occurs during development campaigns when plasma parameters are close to operation limits. Figure 5 shows data for per-pulse disruption frequency in JT-60U during operation with a variety of experimental objectives and discharge parameters [9]. Here q_{eff} is ~ $1.25q_{95}$. Disruption frequency for current flattop is 9.6% (average for 7039 shots). Frequency versus q_{eff} rises slowly to 15% with decrease in q_{eff} from 5 to 3 (q_{95} = 4 to 2.4) Disruptivitiy versus q_{95} evaluated on a per-second basis in Alcator C-Mod and TCV show a similar slowly-rising frequency [10],[11]. Disruption frequency specified for ITER is 10% overall and 30% during plasma development periods.

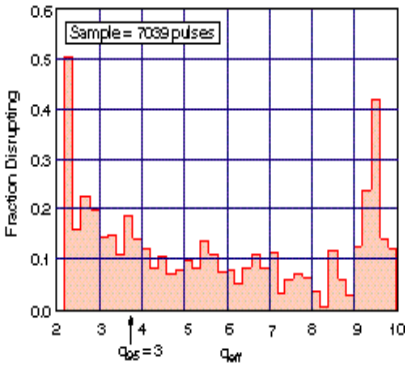

FIG.5. Disruption frequency versus q_{eff} in JT-60U[9].

5. AVOIDANCE OF DISRUPTION

Operation limits obtained from experiments (e.g., l_i limit [12], density limit [13], beta limits [14]) provide a measure of proximity to disruption. For reversed magnetic shear discharges, high pressure gradient at the internal transport barrier (ITB) causes disruption [15], [16]. In JT-60U the ITB pressure gradient has been controlled by toroidal rotation control using co- and ctr-NBI. Temporary degradation of the ITB without reduction of the stored energy is possible: the ITB is then reestablished [17]. This avoids disruptions caused by pressure gradient. When a stable operation region is needed to avoid disruption, a *navigator system* (a state-cognizant/rule-based control system) is useful where many operation limits are present. *Prediction systems* are also beneficial to quantify operational limits and the possibility of impending disruption. Neural network 'disruption indicators' have been demonstrated in DIII-D [18] for β-limit disruption and in ASDEX-Upgrade [19] for density-limit disruption.

6. FAST PLASMA SHUTDOWN

Fast plasma shutdown (in ≤ 1 s in ITER) is needed for reasons that range from mitigation of halo currents during disruptions and VDEs to thermal protection of actively-cooled divertor targets in an ex-vessel loss-of-coolant event. Methods applicable for fast plasma shutdown and/or disruption effect mitigation in ITER have been tested in present tokamaks. However there are significant issues as to how well these methods extrapolate to an ITER/reactor scale plasma.

Reduction of Thermal Quench Heat Flux. Heat flux on ITER divertor targets during thermal quench will be mitigated by the effects of plasma/vapor shielding at the target surface, which will act to redistribute incident energy over the divertor channel surface area (~ 400 m^2). However means to instead deposit the thermal energy (1 GJ) on the 2000 m^2 first-wall surface are desirable. Impurity pellet injection in many tokamaks [20-24] and massive helium gas puffing in DIII-D [25] have demonstrated fast radiation-produced dissipation of the plasma thermal energy with reduced heat flux in the divertor. MHD instabilities characteristic of a disruption are absent in pellet and gas shutdown.

Avoidance of VDE at Current Quench. The radiative plasma cooling produced by impurity pellet injection typically also reduces $I_{h,max}/I_{p0}$ and T_{pf} relative to values obtained following an

equivalent disruption [3]. In certain situations (e.g., following injection or intense gas puffing in JT-60U) a VDE and halo currents can be avoided [5] by positioning the plasma close to the neutral point stability point where toroidal eddy current forces on the after-injection plasma balance [26], [27]. Inward shift of the plasma at thermal quench degrades vertical stability, but this degradation can be reduced by design of the passive structure [28]. However, it is not clear how well neutral-point stability and after-disruption vertical control can be maintained in ITER.

Avoidance and Suppression of Runaway Electrons. In present tokamaks runaway electrons are sometimes produced following disruption or fast shutdown. In ITER, major conversion of plasma current to runaway current by the knock-on avalanche process is projected to occur. However, the effect of MHD fluctuations and/or resistive dissipation of runaway energy by high-density background plasma or neutral gas [29] may offset what could otherwise be a potentially serious problem (surface damage to in-vessel components). Fast shutdown in ITER without runaways by liquid deuterium jet that greatly increases the electron density has been proposed [29], and massive helium gas injection that models this approach has demonstrated in DIII-D [25]. Non-axisymmetric magnetic perturbations can degrade the confinement of relativistic electrons,and thus suppress runaway conversion [30]. In JT-60U, magnetic perturbations enhanced by external helical magnetic fields inhibit runaway electrons during current quench [31]. Even without external helical field, enhancement of magnetic perturbations induced by the impurity pellet injection [24] or due to the decrease in q_{95} below 2 (e.g., VDE) [32] can avoid runaway generation. Slow termination of runaway current is obtained in JT-60U [32], where the toroidal electric field E is positive and possibly lower than the critical field E_C for the avalanche process [33].

These methods hold promise for fast shutdown in ITER plasmas. However, uncertainties, especially the effect of magnetic fluctuations on runaway confinement and the ability to obtain very high plasma densities following disruption or injection (and thus mitigate runaways) make definition of fast but benign plasma shutdown and disruption effect mitigation means for ITER a still-open R&D subject.

References

[1] WESSON, J.A., Nucl. Fusion **30** (1990) 1011.
[2] TAYLOR, P. L., et al., Phys. Rev. Lett. **76** (1996) 916.
[3] GRUBER, O., et al., Proc. of 15th IAEA Conf. Seville 1994, **1** (1995) 675.
[4] ANDREWS, P., et al., IEEE Transactions on Magnetics in press (1998)
[5] NEYATANI, Y., et al., this conference, EXP3/11.
[6] POMPHREY, N., et al., Nucl. Fusion **38** (1998) 449.
[7] CALOUTSIS, A., et al., Nucl. Fusion in press (1998).
[8] PAUTASSO, G., et al., 1998 ICCP combined with 25th EPS, Prague (1998) P2.014.
[9] YOSHINO, R., Disruptivity in JT-60U, #6 ITER D/PC/MHD EG (1996).
[10] GRANETZ, R., Disruptivity in Alcator C-Mod, #6 ITER D/PC/MHD EG (1996).
[11] LISTER, J., Disruptivity in TCV #6 ITER D/PC/MHD EG (1996).
[12] CHENG, C.Z., et al., Plasma Phys. Control. Fusion **29** (1987) 351.
[13] GREENWALD, M., et al., Nucl. Fusion **28** (1988) 2199.
[14] PERKINS, F.W., et al., this conference, ITERP1/11.
[15] ISHIDA, S., et al., Proc. of 24th EPS, Berchtesgarden, **21A, part II** (1997) 489.
[16] OKABAYASHI, M., et al., Nucl. Fusion in press (1998).
[17] YOSHINO, R., Control of ITB to avoid disruption, #9 ITER D/PC/MHD EG (1998).
[18] WROBLEWSKI, D., et al., Nucl. Fusion **37** (1997) 725.
[19] GRUBER, O., et al., Disruption Avoidance, #8 ITER D/PC/MHD EG (1998).
[20] YOSHINO, R., et al., Proc. of 15th IAEA Conf. Seville 1994, **1** (1995) 685.
[21] PAUTASSO, G., et al., Nucl. Fusion **36** (1996) 1291.
[22] KELLMAN, A.G. et al., Proc. of 16th IAEA Conf., Montreal 1996, **1** (1997) 739.
[23] GRANETZ, R.S., et al., Proc. of 16th IAEA Conf., Montreal 1996, **1** (1997) 757.
[24] YOSHINO, R., et al., Plasma Phys. Control. Fusion **39** (1997) 313.
[25] TAYLOR, P., #8 ITER D/PC/MHD EG (1998).
[26] YOSHINO, R., et al., Nucl. Fusion **36** (1996) 295.
[27] NAKAMURA, Y., et al., Nucl. Fusion **36** (1996) 643.
[28] NAKAMURA, Y., et al., Plasma Phys. Control. Fusion **38** (1996) 1791.
[29] ROSENBLUTH, M.N., et al., Nucl. Fusion **37** (1997) 955.
[30] TOKUDA, S., et al., this conference THP2/26.
[31] KAWANO, Y, et al., Proc. of 16th IAEA Conf., Montreal 1996, **1** (1997) 345.
[32] YOSHINO, R., et al., Nucl. Fusion in press (1998).
[33] ROSENBLUTH, M.N., et al., Nucl. Fusion **37** (1997) 1355.